THE JOURNAL OF BIOLOGICAL CHEMISTRY VOL. 282, NO. 48, pp. 34748–34757, November 30, 2007
Printed in the U.S.A.

Quantification and Modeling of Tripartite CD2-, CD58FC Chimera (Alefacept)-, and CD16-mediated Cell Adhesion*

Received for publication, July 9, 2007, and in revised form, September 21, 2007 Published, JBC Papers in Press, October 2, 2007, DOI 10.1074/jbc.M705616200

Michael L. Dustin[‡1], Toby Starr[‡], Daniel Coombs[§], Gerard R. Majeau[¶], Werner Meier[¶], Paula S. Hochman[¶], Adam Douglass[‖], Ron Vale[‖], Byron Goldstein[**], and Adrian Whitty[¶]

*From the [‡]Department of Pathology, New York University School of Medicine and the Program in Molecular Pathogenesis, Helen L. and Martin S. Kimmel Center for Biology and Medicine of the Skirball Institute of Biomolecular Medicine, New York, New York 10016, the [§]Department of Mathematics, University of British Columbia, Vancouver, British Columbia V6T 1Z2, Canada, [¶]Biogen Idec, Inc., Cambridge, Massachusetts 02142, the [‖]Department of Cellular and Molecular Pharmacology, University of California, San Francisco, San Francisco, California 94143, and the **Theoretical Division, Los Alamos National Laboratory, Los Alamos, New Mexico 87545*

Alefacept is a chimeric protein combining CD58 immunoglobulin-like domain 1 with human IgG1 Fc. Alefacept mediates adhesion by bridging CD2 on T cells to activating Fc receptors on effector cells, but the equilibrium binding parameters have not been determined. Alefacept mediated T cell killing by NK cells and adhesion between CD2- and CD16-expressing cells at an optimum concentration of 100 nM. We introduce novel measurements with supported planer bilayers, from which key two-dimensional and three-dimensional parameters can be determined by data fitting. Alefacept competitively inhibited cell bilayer adhesion mediated by the CD2–CD58 interaction. Alefacept mediated maximal adhesion of CD2$^+$ T cells to CD16B, an Fc receptor, in planar bilayers at 500 nM. A mechanistic model for alefacept-mediated cell-bilayer adhesion allowed fitting of the data and determination of two-dimensional binding parameters. These included the density of bonds in the adhesion area, which grew to maintain a consistent average bond density of 200 molecules/μm^2 and two-dimensional association constants of 3.1 and 630 μm^2 for bivalently and monovalently bound forms of alefacept, respectively. The maximum number of CD16 bound and the fit value of 4,350 CD2 per cell are much lower than the 40,000 CD2 per cell measured with anti-CD2 Fab. These results suggest that additional information is needed to correctly predict Alefacept-mediated bridge formation.

Immunoadhesins are biopharmaceuticals that take the basic framework of antibodies and replace the antigen-binding domain with the ectodomain of adhesion molecules (1, 2). The common fragment of IgG (Fc) portion is thought to link to immune effector mechanisms to destroy cancer cells and or over-reactive immune cells. One example of this approach is the drug alefacept, which combines the CD2 binding domain of the adhesion molecule CD58 (LFA-3) with human IgG1 Fc in a single polypeptide chain. Alefacept is approved for treatment of psoriasis. Alefacept mediates reduction of circulating memory T cells in patients and mediates Fc receptor (FcR)[2]-dependent cell-mediated killing of T cells *in vitro* (3, 4). It is hypothesized that alefacept both reduces deleterious effector functions of activated T cells by blocking interaction of CD2 with CD58 and deletes autoaggressive T cells through FcR-dependent killing. When CD16A is the activating FcR each of the individual interactions of alefacept is low affinity with a K_d of 1.5 μM for the CD2–CD58 interaction and K_d of 0.91 μM for the Fc-CD16 interaction (5–8). How these solution affinities relate to interactions in an adhesion area is not clear.

These interactions are proposed to take place in the two-dimensional interface between cells, but there are only limited data on such interactions and no quantitative data on formation of the trimolecular bridges as proposed for alefacept. Determining such parameters in a model system would be a first step to development of a system of two-dimensional pharmacology to better predict *in vivo* behavior in cell-cell contact areas based on *in vitro* measured interaction parameters. Information like affinity and maximum binding has been mainstays of modern pharmacology for over 50 years. The availability of such tools for adhesion mediating drugs would aid in development of effective biological and small molecule drugs based on bridging surface receptor to induce adhesion or cell-cell signaling.

An equilibrium model to predict the ability of immunoadhesins, and related compounds including antibodies, to mediate adhesion would be useful to evaluate current and future pharmaceuticals. The chemistry of these interactions at cell interfaces has been poorly understood due to the technical difficulty of quantifying molecular interactions in cell-cell interfaces. One approach to this problem has been to study the molecular interactions in the hybrid cell-supported planar bilayer system (6, 9, 10). Glass-supported planar bilayers consist of a phospholipid bilayer supported on a layer of water mole-

* This work was supported in part by National Institutes of Health Grants R37-1 AI043542 (to M. L. D.) and R37 GM035556 (to B. G.), Dept. of Energy through contract W-7405-ENG-36 (BG), and a Whitaker Foundation Research Grant (to M. L. D.). The costs of publication of this article were defrayed in part by the payment of page charges. This article must therefore be hereby marked "*advertisement*" in accordance with 18 U.S.C. Section 1734 solely to indicate this fact.

[1] Supported through this work by an Irene Diamond Foundation grant and a research grant from Biogen-Idec. To whom correspondence should be addressed: 540 First Ave. SK2-4, New York, NY 10021. Fax: 212-263-3207; E-mail: dustin@saturn.med.nyu.edu.

[2] The abbreviations used are: FcR, Fc receptor; PBL, human peripheral blood lymphocytes; FITC, fluorescein isothiocyanate; GPI, glycophosphatidylinositol; MR, maximal release; SR, spontaneous release; GFP, green fluorescent protein; BF, bright field; IRM, interference reflection microscopy; D, diffusion coefficient.

cules on a glass, quartz, or SiO_2 surface (11). The bilayer can contain fluorescently labeled receptors and control molecules that are freely mobile in the bilayer. Interaction between these receptors and cell surface molecules in hybrid cell-supported planar bilayer junctions, referred to subsequently as an adhesion area, induces accumulation of the fluorescent receptors and partial exclusion of non-interacting control molecules in the bilayer, which can be detected by fluorescence microscopy. Varying the density of receptors in the substrate enables analysis of adhesion area growth and two-dimensional affinity measurements using the Golan-Zhu method, which makes the assumption that receptor interactions are confined to the adhesion site, while free receptors diffuse over the entire cell surface (6, 12). The interactions of CD2 with CD58 has been studied in detail using supported planar bilayers and the Golan-Zhu analysis revealing a two-dimensional K_d in the range of 1.1–7.6 molecules/μm^2 and a maximal binding (B_{max}) close to the total number of cell surface CD2 accessible by antibodies (6, 12). These results are consistent with self-assembly of an ordered interface into which CD2 diffuses freely. Our hypothesis is that immunoadhesin-mediated adhesion works by similar self-assembly of ordered junctions between cell membranes containing target epitopes and Fc receptors.

In this report we describe a detailed equilibrium model for alefacept mediated adhesion. We test the model by fitting experimental data and derive estimates for key parameters. The model incorporates a growth rule based on constant density of bonds that is well fit by the data. A key prediction of the model is that the concentration of alefacept needed to initiate an adhesion area is inversely proportion to the square of the CD2 density. This prediction is important because it implies that a 5-fold higher expression of a receptor on a target compared with a bystander cell will result in initiation of interaction with the target at 25-fold lower concentration of alefacept than needed to initiate adhesion to the bystander. We experimentally verify this prediction. The data indicate that rules governing access of alefacept-CD2 complexes to the adhesion area are not fully understood and identify areas for further study.

EXPERIMENTAL PROCEDURES

Human Peripheral Blood Lymphocytes (PBL)—In Fig. 1, lymphocytes were separated from freshly drawn peripheral blood (from healthy volunteers employed at Biogen Idec) using Ficoll-hypaque gradient centrifugation, as previously described (3). In Fig. 5 human peripheral blood T cells were obtained from the New York Blood Center (New York, NY). Naive and memory cells were isolated by negative selection with magnetic beads (Miltenyi Biotech, Auburn, CA).

Cells Lines—The $CD16A^+$ $CD2^+$ Jurkat cells used in Fig. 1 were obtained from P. Anderson (Dana Farber Cancer Institute, Boston, MA). The $CD2^+$ CHO transfectants used in Fig. 1 were provided by Cathy Hession (Biogen Idec, Inc. Cambridge, MA) (3). $CD16B^+$ Jurkat cells were obtained from J. Green and E. R. Brown (University of California, San Francisco, CA) (13). Jurkat cells used in Figs. 2–6 were originally obtained from A. Chan (Genentech, S. San Francisco, CA). The gene encoding enhanced green fluorescence protein (eGFP) was fused to the C terminus of a human CD2 cDNA using standard molecular biology techniques, and the resulting fusion construct was verified by sequencing (14). Jurkat cells were transiently transfected with CD2-GFP by electroporation and allowed to recover for 72–96 h prior to imaging.

Alefacept—The fusion protein designated herein as alefacept is composed of the first extracellular domain of CD58 fused to the hinge, CH2 and CH3 domains of human IgG1 (15). For a subset of experiments, to eliminate the possibility that the results might be influenced by aggregated protein that might be present at very low concentrations, the material was further purified by size exclusion chromatography on Superose-6 (Amersham Biosciences). Briefly, 2 ml of alefacept (15 mg/ml) were loaded onto a 1.6 × 100 cm Superose-6 column equilibrated in phosphate-buffered saline at a flow rate of 40 ml/h. Individual fractions were analyzed for aggregate content by analytical size exclusion chromatography using a TSK-3000 column (Toso-Haas, Montgomeryville, PA). Fractions with an aggregate content of <0.5% were pooled, concentrated by ultracentrifugation using YM-30 Centriprep filters (Millipore, Billerica, MA), aliquoted and stored at −70 °C. The final aggregate content was determined to be to be <0.5% after the concentrated pool (12.4 mg/ml) had been put through one freeze/thaw cycle. Molar concentrations of alefacept were calculated with a molecular weight of 72,000.

Alefacept-mediated Adhesion Assay—CHO cells transfected with human CD2 were grown to confluence in wells of flat bottom 96-well plates. Wells were washed twice, and 50 μl of varying concentrations of alefacept were added. Plates were then washed or unwashed as indicated. 10^5 $CD16^+$ Jurkat cells, which were labeled with BCECF-AM according to the manufacturer's directions (Invitrogen-Molecular Probes Inc., Eugene, OR), were then added in 50 μl to wells. Plates were incubated for 0.5 h at 37 °C or 24 °C. Wells were then washed four times. Background signal was that of wells without cells, incubated and washed as were the experimental groups. Total input was the signal released from 10^5 BCECF-AM labeled cells. The percent binding was determined as the (experimental minus background counts) divided by (total input minus background counts) × 100.

Cytotoxicity Assay—Targets were human PBL blasts. Briefly, 10^6 PBL were cultured with 10 μg/ml final concentration of PHA for 3 days. PHA blasts were then collected, washed, 100 μCi of ^{51}Cr was added to 10^7 cells, which were then incubated at 37 °C for 1 h, washed, counted, and resuspended in complete medium. 5×10^3 target cells in 20 μl were added to wells of round bottom 96 well microtiter plates. PBLs freshly prepared from normal donors on the day of the assay were added to the target cells to make a total volume of 200 μl and an effector to target ratio of 50:1. Alefacept was added to wells at the indicated concentrations. Microtiter plates were incubated in a 37 °C, 5% CO_2 incubator for 4 h, centrifuged, and 150 μl of supernatant was removed to measure released ^{51}Cr in a Liquid Scintillation Counter (Wallac Inc., Gaithersburg, MD). Spontaneous release (SR) was counts released from target cells in the presence of medium alone, and maximum release (MR) was counts released from target cells incubated in the presence of 0.5% Triton. Percent lysis was calculated as (experimental minus SR cpm) divided by (MR cpm minus SR cpm). Previously it was shown

that fusion protein mediated cytotoxicity was inhibited by the addition of blocking mAbs specific for CD16 to the 4-h assay cultures. Lysis is dependent on the expression of CD2 by the target cells (3).

Quantitative Flow Cytometry—Flow cytometry experiments were performed on a Becton Dickinson FacsCalibur. FITC labeling of antibodies and determination of the fluoresceine: protein ratio was determined using absorption spectroscopy (16). Calibration was performed using FITC standard beads obtained from Bangs Laboratories (Fishers, IN). Antibody-stained cells were washed twice prior to analysis. Alefacept binding modified from Majeau *et al.* (7). Alefacept was labeled with 0.8 FITC/alefacept. Binding was analyzed by flow cytometry without washing away free alefacept. Because the sample stream does not mix with the sheath fluid prior to reaching the interrogation point there was no alefacept dilution prior to analysis. When the free FITC-alefacept concentration exceeded 100 nM linearity problems were detected with FITC standard beads. To achieve higher concentration of alefacept we then added unlabeled alefacept while keeping the FITC-alefacept at 100 nM. The binding was allowed to reach equilibrium for 5 min at room temperature. Nonspecific binding was assessed after saturating CD2 on the cells with 100 μg/ml of TS2/18. We found that TS2/18 did not dissociate even with high concentrations of alefacept. The fluorescence standard beads were read in parallel at the same concentration of free alefacept to generate a standard curve to determine the number of alefacept molecules bound per cell.

Planar Bilayers—All phospholipids were obtained from Avanti Polar Lipids (Alabaster, AL). Human CD58 was purified from human red blood cells and labeled with FITC while bound to the anti-CD58 antibody TS2/9 (9, 17). Mouse CD48 was labeled with Cy5 (Amersham Biosciences), by a similar procedure, but with OX78 mAb (rat anti-mouse CD48) (18, 19). CD16B was purified from CD16B transfected Jurkat cells using 3G8 mAb (IgG was purified from the hybridoma) and was labeled with Cy3 (Amersham Biosciences) while attached to 3G8 agarose. The CD16B was eluted at pH 3 in a solution with 1% octyl-β-D-glucopyranoside. Planar bilayers composed of 0.4 mM egg phosphatidylcholine (PC) were prepared by detergent dialysis as previously described (9). Bilayers were formed on clean glass coverslips (chromic sulfuric acid for 15 min then rinsed with deionized water, high purity acetone, and dried under a nitrogen stream) in a FCS II flow cell (Bioptechs, Butler, PA). Bilayer formation was initiated by trapping a 1-μl drop or liposome suspension between the coverslip and microaqueduct slide separated by a 250-μm gasket. After 20 min, the flow cell was perfused with 5 ml of Hepes-buffered saline 1% human serum albumin (HBS/HSA; 20 mM Hepes, 1.7 mM K_2HPO_4, 137 mM, NaCl, 5 mM KCl, 5 mM glucose, 1% clinical grade human serum albumin, pH 7.4.). The surface was then blocked with 5% casein in phosphate-buffered saline. After 20 min, the flow cell was again perfused with HBS/HSA.

Imaging—The microscope used to acquire images was equipped with a cooled CCD camera and excitation and emission filter wheels (Yona Microscopes, Silver Spring, MD) (19). The filter set was the XF93 triple band dichroic mirror and individual excitation and emission filters recommended by the manufacturer for FITC, Cy3, and Cy5 dyes (Omega, Burlington, VT). Using this filter set there was no detectable cross-detection of the different dyes in each others filter combinations. A Zeiss ×100 Plan-Neofluar or Neofluar 1.3 NA objective was used for all experiments. Digital images were acquired using IP-Lab software and processed by background subtraction and flat field correction prior to segmentation and analysis of adhesion areas. Bleaching was performed with the focused beam from a Spectraphysics 2.5 W Krypton-Argon laser with wavelength selection using a acoustooptic tunable filter (Solamere Technologies, Salt Lake City, UT).

Single Molecule Imaging of GFP-CD2—Glass-bottomed observation dishes (MatTek Inc., Ashland, MA) were cleaned thoroughly with a 2:1 mixture of concentrated sulfuric acid and 30% hydrogen peroxide prior to use. Cells expressing low levels of CD2-GFP were imaged using objective-type total internal reflection fluorescence excitation on a Zeiss Axiovert 200 M microscope equipped with a Mega-10 ICCD camera (Stanford Photonics, Palo Alto, CA). Cells were treated with 0.5 μM alefacept in HBS, or with HBS alone, and allowed to adhere to glass-bottom observation dishes for 10 min prior to imaging. Movies were then acquired at 30 frames per second in 200-frame bursts during a 10-min period. A suite of particle tracking functions written in the IDL language by John Crocker and colleagues was used to identify trajectories in each image. Short-range diffusion coefficients were determined using Matlab (The MathWorks, Inc., Natick, MA) scripts that perform mean-squared displacement analyses of overlapping, half-second intervals within each trajectory (21).

Adhesion Model—We define the following five equilibrium constants: K_R for the binding of the Fc portion of a ligand (alefacept) in solution to an immunoreceptor (CD16B) on the bilayer; K_E for the binding of one of the CD58 sites of alefacpt to its binding epitope on the CD2 adhesion receptor on a T cell; K_x for the binding of the second CD58 site of alefacept to another CD2 molecule on the same T cell while its Fc site is free; K_{b1} for the binding of alefacept Fc to CD16B when the ligand has one CD58 site bound to CD2; and K_{b2} for the binding of a alefacept Fc to CD16B when the alefacept has both its CD58 sites bound to CD2 on the same T cell. K_x, K_{b1}, and K_{b2} are two-dimensional equilibrium constants while K_R and K_E are three-dimensional.[3]

We use the following notation: L is the alefacept concentration, e_T is the total surface concentration of CD2 when CD2 is uniformly distributed on the T cell; e is the surface concentration of free CD2; e_1 and e_2 are the surface concentrations of alefacept with its Fc portion unbound and with one CD58 site bound and both CD58 sites bound respectively; r_T is the total surface concentration of the CD16B when they are uniformly

[3] K_{b1}, equilibrium constant for binding of alefacept Fc to FcR in planar bilayer when one of alefacept's CD58s is bound to CD2 on the T cell; K_{b2}, equilibrium constant for binding of alefacept Fc to FcR in planar bilayer when both of the alefacept CD58s are bound to CD2; K_E, equilibrium constant for binding of first Alefacept CD58 Ig domain to CD2 on T cell while its Fc site is free; K_R, solution equilibrium constant for binding of Fc to FcR in planar bilayer; K_x, equilibrium constant for binding of second alefacept CD58 Ig domain to CD2 on T cell while its Fc is free; L, alefacept concentration; L_{min}, the minimum concentration of alefacept at which adhesion is observed; L_{max}, the maximum concentration of alefacept at which adhesion is observed; N_T, total number of CD2 per cell.

distributed on the bilayer; r is the surface concentrations of free CD16B and r_1 is the surface concentration of Alefacept bound to CD16B but not bound to CD2; b_1 and b_2 are the surface concentrations of bridging bonds composed of alefacept with one or both CD58 sites bound to the T cell and their Fc site bound to the CD16B on the bilayer. These bridges occur only in the region of closest approach within the adhesion area between a T cell and the bilayer (<15 nm). At equilibrium e, e_1, and e_2 are uniform over the T cell and r and r_1 are uniform over the bilayer. In addition, A is the area of adhesion, A_{cell} is the surface area of the T cell and A_{bl} is the surface area of the bilayer per bound T cell, *i.e.* A_{bl} = (area of the bilayer)/(number of cells bound to the bilayer). We also define $\delta = A/A_{cell}$ *and* $\alpha = A_{cell}/A_{bl}$. From the law of mass action we have that $e_1 = 2K_E Le$, $e_2 = K_E LK_x e^2$, $r_1 = K_R Lr$, $b_1 = 2K_{b1}K_E Ler$, and $b_2 = K_{b2}K_E LK_x e^2 r$.

The following equations allow us to solve for e, r, and δ, in terms of input parameters L, e_T, r_T and α. We can then calculate the concentrations of the two types of bridges, b_1 and b_2, and the adhesion as a function of the ligand concentration. The first two equations arise from the assumption that binding is at equilibrium so that the total numbers of CD2 and CD16B are constant. There is negligible depletion of alefacept in our experiments so L is known. The third equation describes how the adhesion changes with bridge concentration. It postulates that the adhesion area grows with the number of bridging bonds by keeping the bond density constant (22). From Equations 1–3, the bridging bond density and adhesion area were calculated and fit simultaneously to the data,

$$e_T = e + e_1 + 2e_2 + \delta(b_1 + 2b_2) \quad \text{(Eq. 1)}$$

$$r_T = r + r_1 + \alpha\delta(b_1 + b_2) \quad \text{(Eq. 2)}$$

$$\beta = b_1 + b_2 \quad \text{(Eq. 3)}$$

where b_1 and b_2 are the surface concentration of alefacept with one or both CD58s bound to CD2 on the T cell and its Fc bound to FcR on the planar bilayer. e_1 and e_2 are the surface concentration of alefecept with one or both CD58 sites bound to CD2 and its Fc portion free. r is the surface concentrations of free CD16B and r_1 is the surface concentration of Alefacept bound to CD16B but not bound to CD2. r_T is the surface concentration of FcR on bilayer prior to cell interaction.

RESULTS

Quantitative Analysis of Alefacept-induced NK Cell-mediated T Cell Killing and Cell-Cell Adhesion—Alefacept-mediated killing of CD2-positive T cells by NK or similar cells can be demonstrated using an *in vitro* assay (3), but the optimal alefacept concentration was not determined. Human peripheral blood NK cells killed human T cell blasts in the presence of nanomolar to micromolar concentrations of alefacept (Fig. 1*A*). The concentration of alefacept that gave maximal killing was 100 nM, but significant killing was triggered at 1 nM. High concentrations of alefacept (>1 μM) inhibit the killing reaction (Fig. 1*A*). This is expected because saturation of the CD2 and CD16A receptors by separate alefacept will inhibit formation of the CD2/alefacept/CD16A bridges between NK cells and CD2$^+$ target cells. The physical formation of such bridges by alefacept is also revealed in a monolayer adhesion assay in which CD16A expressing Jurkat cells adhere to CD2 expressing CHO cell monolayers only in the presence of alefacept (Fig. 1*B*) (23). Adhesion is observed at 1 nM alefacept and is decreased at >1 μM alefacept (Fig. 1*B*). However, the number of bridges that mediate killing or adhesion cannot be deduced from either of these results.

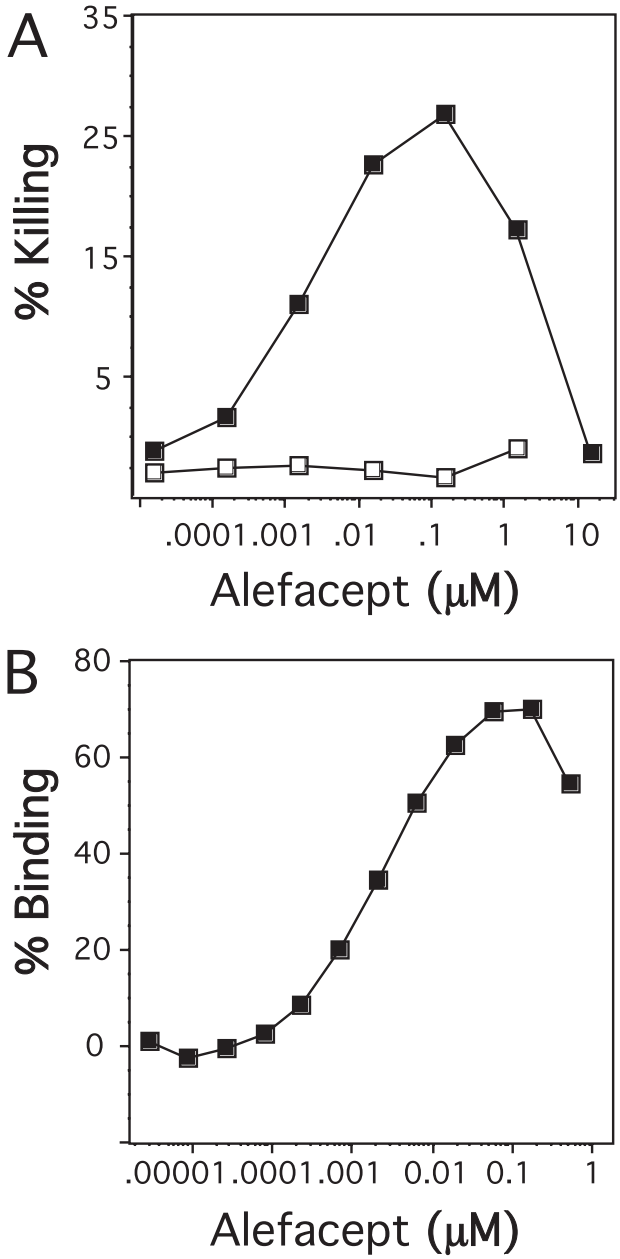

FIGURE 1. **Quantitative analysis of alefacept-mediated effector function and adhesion.** *A*, human PBL, a source of NK cells, were incubated with 5×10^3 ^{51}Cr-labeled PHA-blasted allogeneic PBL (Effector:Target ratio of 50:1) in the presence or absence of alefacept (*filled squares*) or human IgG (*open squares*) as indicated for 4 h in a cytotoxicity assay. *B*, monolayers of CHO transfectants expressing human CD2 were incubated with indicated concentrations of alefacept. BCECF-AM labeled CD16A$^+$ Jurkat cells were then added and incubation continued. Wells were then washed, and plates were read at 485 nm to determine the percentage of cell binding. Results are representative of three experiments.

Inhibition of CD2–CD58 Interaction in Jurkat T cell-Bilayer Interface by Alefacept—We first wanted to determine if alefacept is a competitive inhibitor of CD2–CD58 interactions, or if the inhibition process in the two-dimensional interface is more complex. Cells expressing CD2 can adhere directly to supported planar bilayers containing its ligand CD58 (17). The effect of alefacept on the direct interaction of CD2 and CD58 was quantified by imaging adhesion area between CD2-positive Jurkat T leukemia cells and supported planar bilayers containing Cy3-labeled CD58, which is naturally GPI-anchored and thus laterally mobile in the bilayer. Each data point was based on imaging ~100 adhesion areas. Four images were acquired for each data point: bright field to detect the cell, interference reflection microscopy (IRM) to detect close juxtaposition of the T cell and planar bilayer membranes, Cy3 fluorescence to measure the density of CD58 within and outside the adhesion area and Cy5 fluorescence to measure the exclusion of the non-interacting control protein CD48 from the adhesion area (Fig. 2*A*). The density of CD2–CD58 interaction is calculated taking the total amount of CD2 in the adhesion area and subtracting the CD58 density outside the adhesion area after multiplying by the ratio of the free CD48 in the same contact over the free CD48 outside the same adhesion area. We find consistently that the adhesion areas have ~30% less CD48 than the surrounding bilayers. The two-dimensional K_d values, describing the apparent affinity of the CD2/CD58 interaction in the two-dimensional environment of the adhesion area, and B_{max} values, indicating the maximum number of complexes formed without and with alefacept were calculated using Golan-Zhu plots (12, 19) (Fig. 2*B*). Even at 5 μM alefacept adhesion and CD2–CD58 interactions were detected and two-dimensional K_d and B_{max} could be determined (Fig. 2*B*). The value of B_{max} did not vary significantly over a range of alefacept concentrations (Fig. 2*C*). The IC_{50} of alefacept for decreasing the two-dimensional K_A was 50 nM (Fig. 2*D*). Direct binding of FITC-alefacept to Jurkat cells was also determined, and the K_{App} was 0.1 μM, similar to the IC_{50}. Because we have previously determined the monovalent binding of CD58 to CD2 has a K_d of 1.5 μM (19), it is likely that the K_{app} and IC_{50} of alefecept reflect mainly bivalent binding to CD2. The maximum number of bound alefacept in this concentration range was ~20,000 or half the number of CD2 as indicated by anti-CD2 Fab binding (see below), also consistent with bivalent binding. Thus, alefacept acts as a simple competitive inhibitor of CD2–CD58 adhesive interactions.

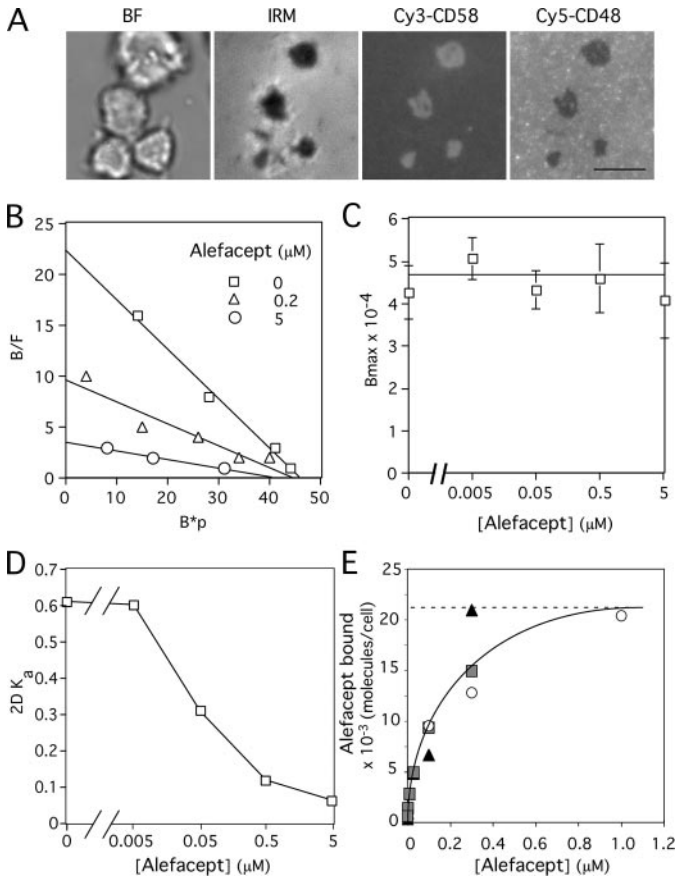

FIGURE 2. **Alefacept competitively inhibits two-dimensional CD2–CD58 interaction.** *A*, images of CD2-mediated adhesion of Jurkat T cells to a planar bilayer containing GPI-linked Cy3-CD58 and the non-interacting control protein Cy5-CD48. 250 molecules/μm^2 Cy3-CD58 ligand; 250 molecules/μm^2 Cy5-CD48 control. *Scale bar*, 10 μm. *B*, Golan-Zhu plots of binding data for Jurkat T cell adhesion to planar bilayers containing CD58 interaction in the presence of 0, 0.2, or 5 μM alefacept. Each point represents the average value for at least 100 cells. The negative reciprocal of the slope gives the apparent two-dimensional K_d, and the x-intercept multiplied by 800 (cell surface area) gives the maximal number of complexes that form at saturating CD58. *C*, B_{max} values for CD2/CD58 interaction in adhesion areas as a function of soluble alefacept concentration. *D*, values of the two-dimensional K_a for CD2/CD58 interaction in adhesion areas as a function of alefacept concentration. Values are mean of three experiments where each point in the Golan-Zhu analysis represents mean of greater than 100 cells. *E*, FITC labeled aggregate free alefacept was incubated with Jurkat T cells for 5 min at 24 °C and then the cells were analyzed on a flow cytometer without washing. The number of alefacept bound per cells was calibrated with fluorescent standard beads. Points represent data from three experiments converging on 20,000 alefacept bound per Jurkat cell.

Effect of Alefacept on CD2 Lateral Mobility in Jurkat Cells—The data above suggest that alefacept binding to CD2 does not hinder its access to the adhesion area. To more directly address the impact of alefacept binding on CD2 dynamics we determined CD2 lateral mobility with and without bound alefacept by single particle tracking. Single CD2-GFP molecules, expressed by electroporation of a plasmid encoding this molecule into Jurkat cells, were tracked over several seconds to determine the average diffusion coefficient (D). In the absence of alefacept, D was 0.16 $\mu m^2/s$ (Fig. 3*A*), which is 2-fold faster than the D measured with bivalent antibodies by fluorescence photobleaching (24). When the cells were treated with 0.5 μM alefacept for 10 min at 24 °C prior to measurement, D was 0.065 $\mu m^2/s$, a 2.5-fold reduction (Fig. 3*B*). GFP adsorbed to glass has an apparent D of 0.03 $\mu m^2/s$ because of noise in the fluorescence, which is interpreted by the tracking algorithm as centroid movement. When this threshold is applied the mobile fraction of CD2-GFP is 87% in the absence of alefacept and 62% in its presence. Thus the immobile fraction cannot exceed 13 or 38% in the absence or presence of alefacept binding, respectively.

Visualization of Alefacept-mediated Interactions in Jurkat T Cell-Bilayer Interface—Alefacept was tested for the ability to form tripartite interactions (bridges) between CD2 on the surface of Jurkat cells to Cy3-CD16B on supported planar bilayers. CD16B is naturally glycophosphatidylinositol-anchored (25), which made it ideal for presentation in the supported bilayers in a laterally mobile form. Jurkat cells did not form adhesion areas

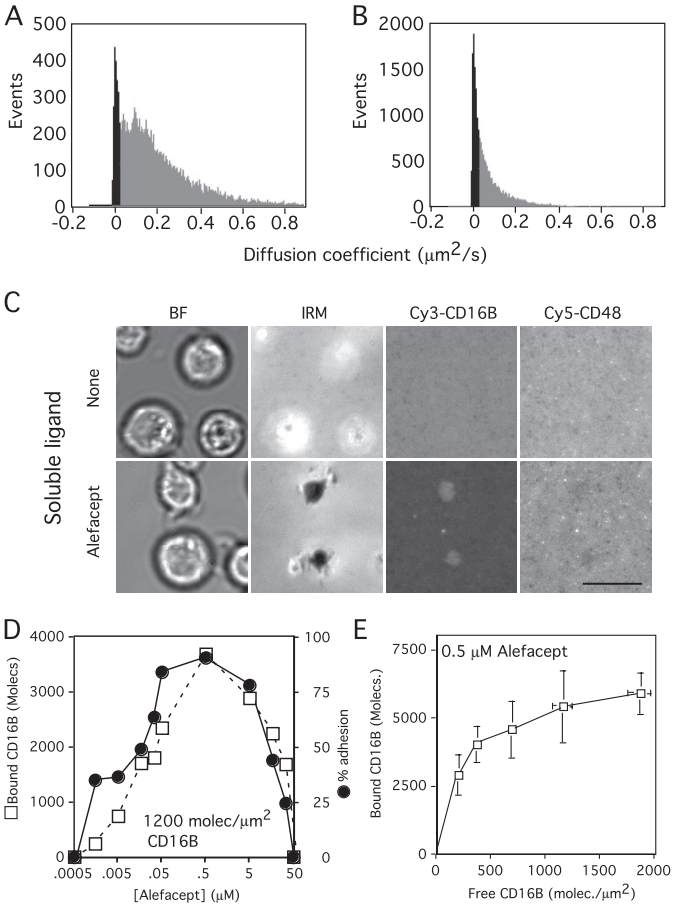

FIGURE 3. **Alefacept effect on CD2 lateral mobility and adhesion formation.** *A*, single molecule analysis of short range diffusion of CD2-GFP on untreated Jurkat cells. $n = 716$ particles, D = 0.18 $\mu m^2/s$. The *black area* includes all events that may be "immobile" in that their movement is less than or equal to that of GFP attached to glass, whereas the *gray area* includes particles with greater diffusion that GFP attached to glass. By this criterion 87% of the particles are unambiguously mobile. *B*, short-range diffusion analysis on cells treated with 0.5 μM alefacept. $n = 827$ particles. D = 0.08 $\mu m^2/s$. By the criteria applied in *C*, 62% of the particles are mobile. Data are representative of two experiments. *C*, images of alefacept-mediated bridging of CD2-expressing Jurkat T cells to a planar bilayer containing GPI-linked Cy3-CD16B. 600 molecules/μm^2 CD16B; 250 molecules/μm^2 CD48. The soluble ligand is buffer control or 0.5 μM alefacept. *Scale bar* = 10 μm. *D*, titration of alefacept with CD16B bilayers (1200 molecule/μm^2). Amount of bound CD16B in the interface (*open squares*) and percent adhesion (*filled circles*) at indicated concentrations of soluble alefacept. Each point represents the mean of greater than 100 adhesion areas. *E*, titration of CD16B density in the bilayer at the optimal concentration of alefacept (0.5 μM). Each point is a mean of six experiments in which each data point is determined by greater than 100 Jurkat cell adhesion areas.

detectable by IRM on CD16B containing bilayers in the absence of alefacept. However, when alefacept was included adhesion areas were detected by the dark IRM, by the accumulation of Cy3-CD16B, and by exclusion of Cy5-CD48 (Fig. 3*C*). It was notable that CD48 was less excluded from the alefacept-mediated contacts than from CD2–CD58-mediated contacts. The density of bridges was calculated as the total Cy3-CD16B density in the adhesion area minus the Cy3-CD16B outside the adhesion area after multiplying by the ratio of Cy5-CD48 inside and outside the same adhesion area. We first fixed the CD16B density at 1200 molecules/μm^2 and varied alefacept from 0.5 nM to 50 μM. The formation of adhesion areas showed a bell-shaped dependence on alefacept concentration similar to that seen in the killing and cell adhesion assays shown in Fig. 1, although the bell shape curve was shifted one log toward higher alefacept concentrations. The percentage of cells forming adhesions and the number of bridges were maximal at 0.5 μM alefacept and were lost completely at 25 μM alefacept, but could be detected at alefacept concentrations as low as 1.5 nM (Fig. 3*B*). The roughly bell-shaped curve was asymmetric with extended adhesion formation and bridge number at low concentrations of alefacept in the 1.5–50 nM range. Similar results were obtained when the initial CD16B density in the bilayer was 600 molecules/μm^2 (not shown). We titrated CD16B at 0.5 μM alefacept and found that the system appeared to be nearing saturation at ~5000 CD16B accumulated per adhesion area (Fig. 3*C*).

Mechanistic Model for Alefacept-mediated Adhesion—To achieve a more quantitative understanding we next developed a mathematical model that could be used to test our mechanistic hypothesis against the experimental data and probe the influence of different factors on the efficiency of adhesion. The equilibrium model incorporates all 7 reactions that describe the possible monovalent and bivalent binding of alefacept to CD2, the monovalent binding of alefacept to CD16B and two types of bridges that can form (Fig. 4*A*). In the model we fix the values of equilibrium constants ($1/K_d$) for IgG Fc binding to CD16B (K_R), for monomeric CD58 binding to CD2 (K_E), and for binding of the second CD58 moiety in alefacept to CD2 after binding of the first CD58 to the same cell has already occurred (K_X). The equilibrium constants K_{b1} and K_{b2} for the binding of the $CD2_1$-alefacept and $CD2_2$-alefacept complexes to CD16B, the bridging density β, and the total number of CD2 on the cell were varied to fit the model parameters to the data. The model was used to fit alefacept titrations at 1200 and 600 molec./μm^2 of CD16B (Fig. 4, *B* and *C*). The best fit values of K_{b1} and K_{b2} were 3.1 μm^2 and 630 μm^2, respectively (Fig. 4, *B* and *C*). The total number of CD2 per cell was fit at 4,350, only about 10% of the total amount of CD2 known to be on the cell surface. At low alefacept concentration, most alefacept are bound to two CD2, but as the alefacept concentration is increased most alefacept bind only a single CD2 (Fig. 4, *B* and *C*). The mechanism of adhesion area growth in the model is a balance between adhesive energy and repulsive and mechanical forces that limit adhesion area. The fit value for β, the density of bonds in the adhesion area, was 200 molecules/μm^2 (Fig. 4*D*). An important prediction of the model is that the alefacept concentration required for formation of an adhesion $(L_{min})^3$ varies inversely with the square of the CD2 density (Fig. 4*E*). This result predicts that alefacept should be highly discriminative with respect to differences in CD2 density.

CD2 Density and Alefacept-mediated Adhesion of Normal Human T Cells—CD2 expression is higher on human memory cells than on naive cells when measured at the single cell level by flow cytometry (26). We tested the hypothesis that differences in the level of CD2 expression on naive, memory, and recently activated effector cells would lead to different thresholds for adhesion as a function of alefacept concentration. Flow cytometry with directly conjugated FITC-anti-CD2 mAb determined that memory T cells have 1.46 ± 0.11-fold more CD2 than naive T cells (Fig. 5*A*). Effector T cells expressed 5.3 ± 1.3-fold

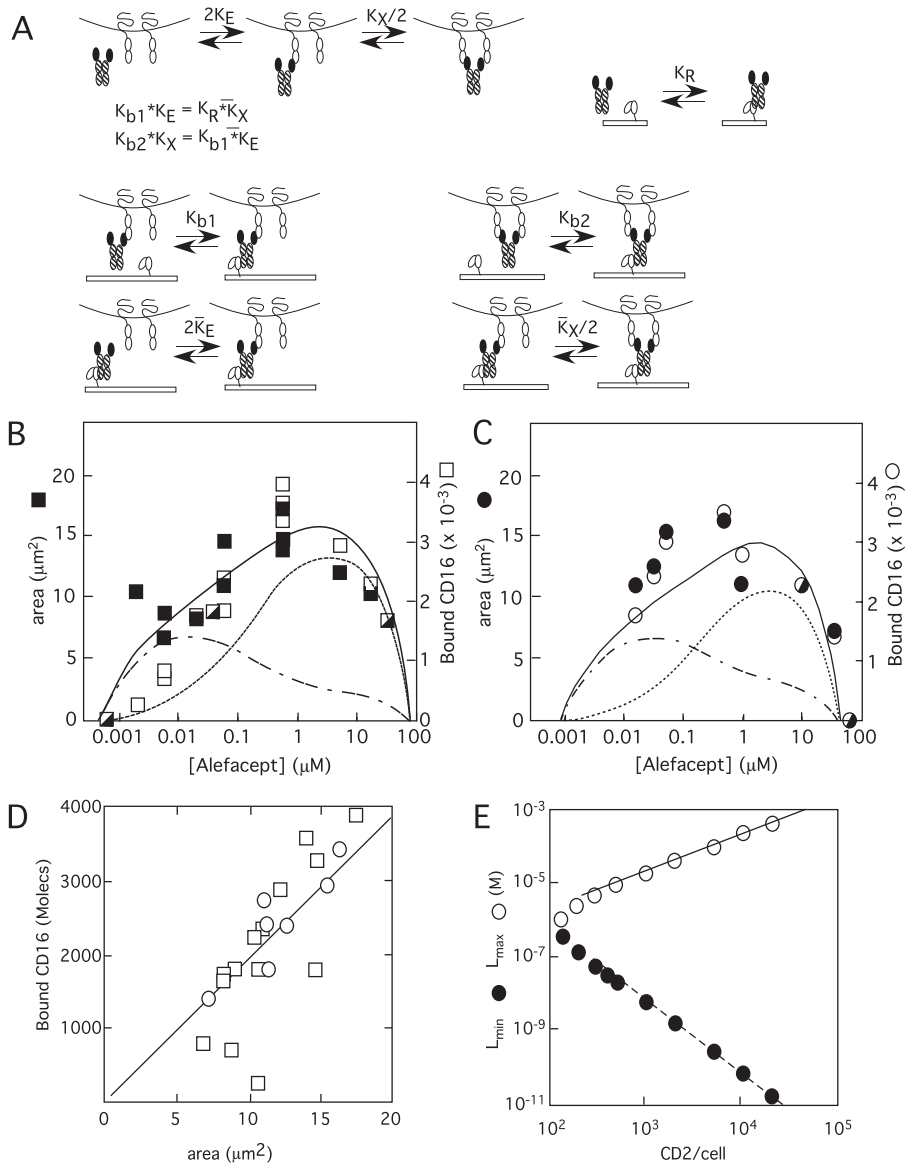

FIGURE 4. **Fitting of data to a model for immunoadhesin-mediated bridge formation.** *A*, mechanistic steps in immunoadhesin-mediated adhesion. The 7 reaction steps considered in the bivalent model and the relationships that must be satisfied based on the law of detailed balance (equations shown). *B* and *C*, CD16B binding under conditions where the initial CD16B density equals 1200 molecules/μm^2 (*B*) and 625 molecules/μm^2 (*C*). Each data point is determined by greater than 100 Jurkat T cell adhesion areas in which the area (*filled symbols*) and bound CD16 number (*open symbols*) was measured. In the model, the density of bridges in the adhesion area is constant ($\beta = B/A$). The *solid lines* in *B* and *C* are the simultaneous fit of the model to the area and bound CD16 data at the two CD16B densities using nonlinear least squares regression based on a finite difference Lenvenberg-Marquardt algorithm. The model predicts that bivalent alefacept-CD2 interaction dominates a low alefacept concentration (*dot-dash-dash line*), while monovalent binding dominates at higher alefacept concentration (*dashed line*). In the fit the following parameters were held constant: $A_{cell} = 800\ \mu m^2$, $K_E = 6.7 \times 10^5\ M^{-1}$, $K_R = 1.3 \times 10^6\ M^{-1}$, and $K_x = 0.033\ \mu m^2$. The best fit values of the four parameters that were varied were: $\beta = 200$ molecules/μm^2, $K_{b1} = 3.1\ \mu m^2$, $K_{b2} = 630\ \mu m^2$, and $N_T = 4{,}350$ CD2 per cell. A reasonable fit could not be obtained if we fixed $N_T = 40{,}000$ CD2 per cell. *D*, straight line fit of bound CD16B *versus* adhesion area. Data for bilayers containing initial CD16B density of 1200 molecules/μm^2 (*squares*) or 625 molecules/μm^2 (*circles*) corresponding to data in *panels B* and *C*. Simple linear regression sets $\beta = 190$ molecules/μm^2, close to the fit of 200 molecules/μm^2 that takes into account all model parameters. *E*, predictions of L_{min} and L_{max}. Symbols are calculated values. The *solid line* has a slope of 1, and the *dashed line* a slope of -2 indicating that L_{max} is directly proportional to the CD2 density and that L_{min} is inversely proportional to the square of the CD2 density. Note that the model predicts that below 320 CD2 per cell there is no alefacept concentration at which adhesion occurs.

greater levels of CD2 compared with naive T cells (Fig. 5*A*). If the amount of CD2 measured by flow cytometry is related to the density of CD2 on the cell surface then the expected difference in alefacept required to initiate adhesion should be 2.2- and 25-fold lower for memory cells and effector cells compared with naive T cells, respectively. Surprisingly, adhesion analysis with different concentrations of alefacept at a fixed concentration of CD16B (500 molecules/μm^2) did not detect any difference in adhesion between naive, memory, and effector cells, or the Jurkat T cell line, over the entire range of alefacept concentrations (Fig. 5*B*). Because these cells all express different amounts of CD2 we considered that the surface areas were proportional to CD2 amount such that CD2 density would not vary. We analyzed the relative cell size by flow cytometry using forward angle light scattering, which is proportional to size. Effector T cells were much larger than naive T cells, as expected (Fig. 5*C*). Unexpectedly, we observed that memory cells are larger than naive T cells (Fig. 5*C*). While these results do not allow a precise calculation of the surface density, this data along with the adhesion results suggest that the larger amounts of CD2 on memory and effector T cells maintains an invariant CD2 density on the surface of T cells at different stages of differentiation, including the transformation events involved in generation of the Jurkat tumor cells. Therefore, it seems likely that the control of the CD2 transcription and/or translation is linked to cell growth.

Adhesion Initiation and CD2 Density—To test the prediction of the model that $L_{\min}$ varies inversely with the square of the CD2 density, we needed a different way to obtain cells with different levels of CD2. We accomplished this by blocking a proportion of the CD2 on the surface with a monovalent Fab derived from the high affinity anti-CD2 Ab TS2/18. We determined the concentration of TS2/18 Fab that blocked 80% of the CD2 on Jurkat (Fig. 5*D*). Once bound, the TS2/18 Fab was stable for over an hour after washing away excess Fab without or with 1 μM alefacept present (data not shown). We then tested adhesion of Jurkat cells with 100 or 20% of the normal level of free CD2 to bilayers with CD16B and found that we needed 25-fold more alefacept to

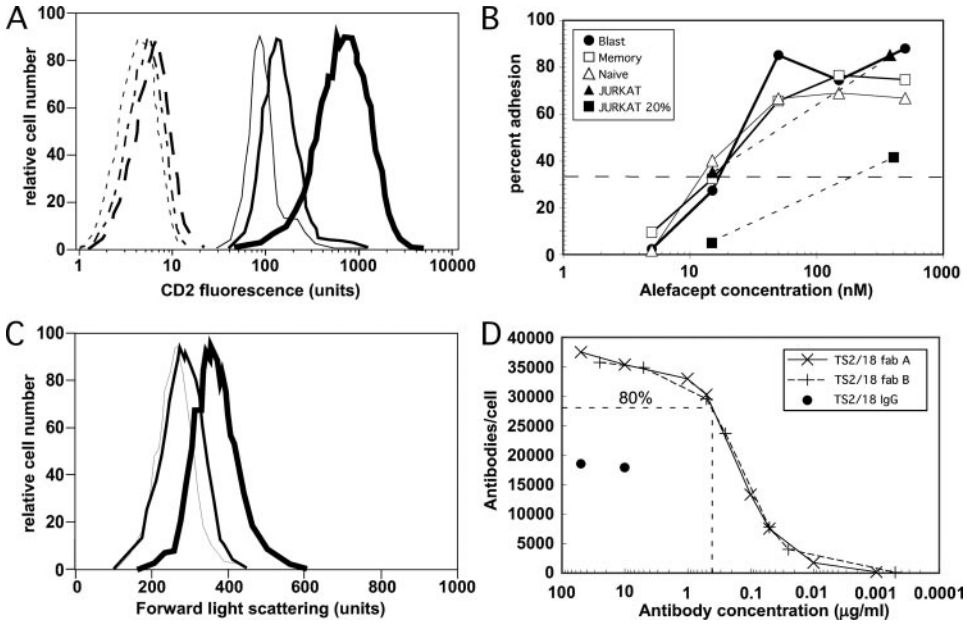

FIGURE 5. **CD2 expression and alefacept-mediated adhesion.** *A*, peripheral blood T cells were separated into naive and memory populations using appropriate MACS kits to obtain >90% pure populations. Cells were stained with saturating concentrations of FITC-TS2/18 (*solid lines*) or control antibody FITC-YN1/1 (*dashed lines*), washed, and analyzed. Naive (*1× thickness line*), memory (*2× thickness line*), and effector (*3× thickness line*) were analyzed and calibrated to IgG bound using FITC calibration beads and antibody F:P ratios. Data are representative of three experiments. *B*, percent adhesion was analyzed with naive T cells (*open triangles*), memory T cells (*open squares*) or *in vitro* activated T cell blasts (*filled circles*) on planar bilayers containing 500 molecules/μm^2 CD16B and the indicated concentration of Alefacept at 24 °C for 60 min. In separate experiments plotted on the same graph, adhesion of Jurkat cells (*filled triangles*) or Jurkat cells with 80% of CD2 blocked by TS2/18 Fab (*filled squares*) to bilayers with 500 molecules/μm^2 CD16B was measured at two concentrations of alefacept spanning a 25-fold range. Adhesion was scored by interference reflection microscopy and bright field microscopy and confirmed by evaluation of CD16 fluorescence in the adhesion area. At least 10 fields were analyzed with greater than 200 input cells. Symbols are listed in legend. Data are representative of three experiments for each point. *C*, forward scatter analysis for cell populations analyzed in *A*. Data are representative of three experiments. *D*, titration of TS2/18 Fab (x and + symbols are two Fab preps) to determine the concentration needed to block 80% of CD2 molecules (*dashed lines*). "Saturation" binding of TS2/18 IgG (*filled circles*) is shown for comparison. Data are representative of three experiments.

compensate for a 5-fold reduction in CD2 density at an adhesion percentage of 35% (Fig. 5*B*, *triangles*). While we examined a limited number of data points within this range, we have obtained the same result in three independent experiments, each with over 100 adhesion sites analyzed.

Distribution of Free CD2 Is Consistent with Contact Area Measurements—The data in Fig. 2 and 4 predict that the amount of CD2 translocated to the Jurkat cell-bilayer interface should be much greater on bilayers containing 200 molecules/μm^2 CD58 compared with 1 μM alefacept and bilayers containing 500 molec/μm^2 CD16B. To test this in a different manner we hypothesized that the free CD2 density measured on membrane areas not in contact with the substrate should be lower on Jurkat cells contacting the CD58 containing bilayers compared with Jurkat cells adhered to the CD16B bilayers via alefacept. We performed confocal microscopy analysis using an Fab of the non-blocking anti-CD2 antibody CD2.1 (27) to test this hypothesis by a different method. Confocal scans for cells with similar contact area size revealed that 35% of CD2 on the Jurkat cell in contact with bilayers containing CD58 remained on non-contact surfaces compared with 73% of CD2 on the Jurkat cells in contact with bilayers containing CD16B in the presence of alefacept (Mann-Whitney test, $p < 0.001$; Fig. 6, *A* and *B*). This result was quantitatively consistent with the prediction of Figs. 2 and 4.

Inhibition of Bridge Formation by Soluble IgG—Another prediction of the model was that physiological concentrations of human IgG would inhibit adhesion. We tested this by adding purified human IgG (with isotypes representative of human plasma) to adhesion experiments with Jurkat cells, planar bilayers with 600 molecules/$\mu m^2$of CD16B and 0.5 μM alefacept. The concentration of human IgG in blood plasma is ~10 mg/ml and in tissues interstitial fluid is ~3 mg/ml. Adhesion was highly efficient in the absence of human IgG and was reduced significantly by 1 mg/ml human IgG and was eliminated at 10 mg/ml human IgG (Fig. 6*C*). Interestingly, significant, but reduced, adhesion was detected at 3 mg/ml human IgG (Fig. 6*C*). Thus, the adhesion reaction is likely to be attenuated *in vivo* and immunoadhesin-mediated adhesion should be more favorable in tissues with lower interstitial IgG concentration.

DISCUSSION

An important potential mechanism for biopharmaceuticals is to bring about interactions between cellular proteins either within a cell (*cis*) or between two cells (*trans*). It has been proposed that a number of drugs, such as alefacept (3), Campath-1H (Alemtuzumab) (28), anti-Erb2 (Trastuzumab) (29), anti-CD20 (Rituximab) (30), and anti-TNF (Infliximab) (31), act, at least in part, by bridging surface epitopes of one cell to CD16 or CD64 on monocyte/macrophages resulting in deletion of the targeted cell (32), particularly in the liver (33). Alefacept may be more dependent on this mechanism because the low affinity of its CD2 binding domain confers relatively low potency as a competitive inhibitor of CD2–CD58 interaction, and thus likely makes this agonistic activity on FcR-positive cells the most efficient mode of action. We have quantified alefacept activity using interaction between T cell leukemia cell lines expressing CD2 and/or primary human T cells and artificial supported planar bilayers containing either CD58 (inhibition) or CD16B (adhesion). This approach makes it possible to obtain quantitative data on molecular interactions that would be difficult or impossible to measure with cell-cell systems. While alefacept can competitively inhibit the two-dimensional interaction of CD2 and CD58 with a K_i ~50 nM, it is more potent in mediating bridging between CD2 and CD16B, this effect being seen at >3 nM alefacept.

These results help explain how an immunoadhesin that relies for its therapeutic activity on interactions that individually are

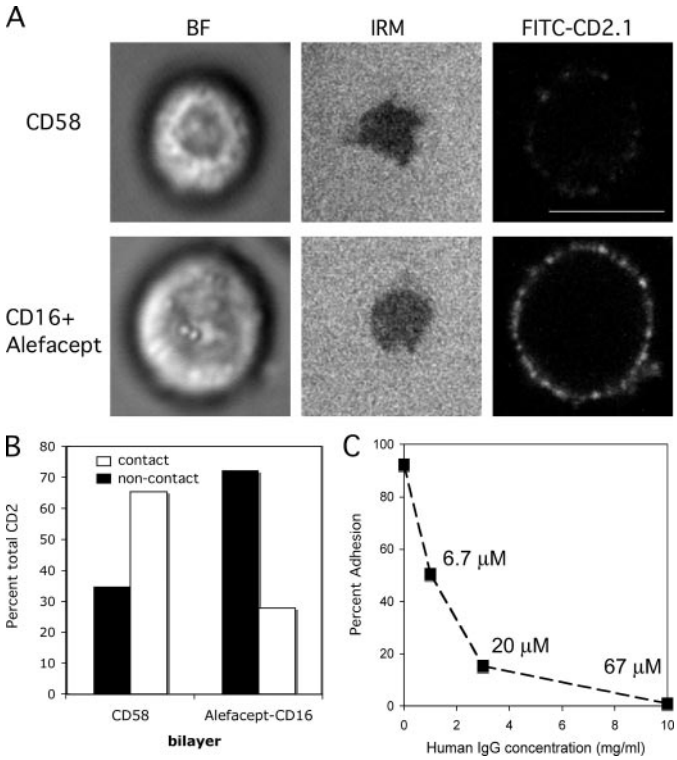

FIGURE 6. **CD2 distribution and inhibition by soluble IgG.** *A*, Jurkat T cells were stained with FITC-CD2.1 Fab and allowed to interact with planar bilayers containing 200 molecules/μm^2 CD58 or 500 molecules/μm^2 CD16 in the presence of 1 μM alefacept. Confocal microscopy was used to obtain a BF image, an IRM image, and a 488-nm laser excitation, 530/30-nm band pass confocal scan through the middle of the cell (FITC-CD2.1). The faint signal from the cell on CD58 indicates extensive redistribution of CD2 to the interface. *Scale bar* = 10 μm. *B*, percent CD2 loss from the cells was determined for 100 cells in each condition relative to FITC-CD2.1 Fab-labeled Jurkat cells adhering to CD80, which does not induce any reorganization of CD2, to determine, which was used to obtain the 100% value. The "non-contact" value was directly measured and the "contact" value was calculated based on the assumption that all CD2 lost from the non-contact surface is located in the interface. *C*, Jurkat T cell adhesion to supported planar bilayers containing 450 molecules/μm^2 CD16B at 500 nM alefacept and the indicated concentration of protein A-purified human IgG. Adhesion was scored by interference reflection microscopy and bright field microscopy and confirmed by evaluation of CD16 fluorescence in the adhesion area. At least 10 fields were analyzed with greater than 200 input cells. Data are representative of three experiments.

weak can mediate specific cell-cell interactions to give low nanomolar potency in *in vitro* cell-based assays as well as high efficacy *in vivo*. Our results suggest that adhesion will be most efficient in tissues with lower interstitial IgG and less efficient in plasma where soluble IgG will compete for binding to Fc receptors. This depends upon the affinity of the Fc receptor for IgG1. Published values for CD16A are in the range of 1 μM, whereas values for CD16B range from 1 to 30 μM (8, 34). While we have not directly measured the affinity of IgG1 Fc to the CD16B purified from Jurkat cells, we can only fit our adhesion (Fig. 4) and soluble IgG inhibition data (Fig. 6) using $K_R > 0.5 \times 10^6$ M^{-1}. The value $K_R = 1.3 \times 10^6$ M^{-1} corresponding to that measured by Galon *et al.* gives an excellent fit of the adhesion data. The optimal concentration for CD16A-mediated cell-cell adhesion is 10-fold lower than for CD16B-mediated cell-bilayer adhesion. This suggests that the affinity of CD16A expressed on these cells is higher than the affinity of CD16B for the IgG Fc of alefacept.

A caveat of the supported planar bilayers system as a model for cytotoxic cells *in vivo* is that while FcR diffuse freely in a homogeneous dissordered planar bilayer, FcR in cytotoxic cell membranes are likely subject to preclustering because of cytoskeletal interactions and inhomogenous membrane domains (35). Furthermore, cytotoxic T cells use other adhesion molecules like LFA-1 to hold cells together and thus the alefacept interactions would not need to mediate adhesion alone. Nonetheless, it is noteworthy that killing and cell-cell adhesion are most efficient in the alefacept concentration range leading to bivalent alefacept-CD2 interaction. This suggests that the bivalently bound CD2, which is less mobile, maybe more efficient at triggering killing and active modes of adhesion.

The model only provided a good fit when the total number of CD2 on the cell was set to a relatively small value of ~4350 molecules compared with the measured value of 40,000. Because the model explicitly treats competition with soluble alefacept some other process must account for the relatively small number of CD16B that are accumulated at saturation for CD16B with optimal alefacept concentration. Alefacept-mediated inhibition of CD2–CD58 was competitive such that there was no evidence for alefacept directly decreasing movement of CD2 to the contact area when alefacept was not engaged by an FcR. Alefacept binding decreased CD2 lateral mobility more than would be expected based upon dimerization alone (36), but reduced rate of mobility should not alter the equilibrium recruitment. Direct measurement of CD2 distribution on cells during alefacept mediated adhesion is consistent with recruitment of only 27% of CD2 to the interface, which is consistent with the requirement for less CD2 to fit the data to the model. There are a number of previously described membrane cytoskeletal processes that could account for this exclusion of alefacept-CD2 complexes from the adhesion area when alefacept is engaged by an FcR. One possibility is that when alefacept engaged CD2 is further oligomerized by binding to CD16B, this may immobilize a large fraction of CD2 outside the adhesion area via global effects on membrane cytoskeletal association, an effect previously described as anchorage modulation (37). Another possibility is that the interaction of alefacept-CD2 complexes with CD16B in the bilayer may create a diffusion barrier at the outer edge of the adhesion area such that mobile alefacept-CD2 complexes would still be excluded. Such cell surface diffusion barriers in the absence of anatomical features like tight junctions have been described (38). Either of these processes would suggest a partial activating signal being transduced by CD2, for which there is significant precedent (39).

The adhesion area growth rule applied in this model is similar to that utilized by Shao *et al.* (40) for the CD2–CD48 interaction. The average bond density in the CD2–CD48 adhesion areas was ~800 molecules/μm^2, whereas that for the Alefacept-mediated bridge formation is ~200 molecules/μm^2. The bimolecular CD2–CD58 interaction may require a higher bond density to mediated adhesion than the trimolecular CD2/alefacept/CD16B interaction because the small bimolecular complex may need to overcome greater repulsive forces associated with close membrane approach than the more extended trimolecular interaction (22).

The model predicts that the concentration of immunoadhesin needed to initiate adhesion will vary inversely with the square of the antigen density. This is a direct consequence of the avidity effect associated with bivalent binding of the two Fab (20). We tested this prediction directly by using anti-CD2 Fab to effectively reduce CD2 density 5-fold without changing other attributes of the cell, and found that a 5-fold decrease in epitope expression indeed led to a need to increase by ~25-fold the concentration of alefacept required for adhesion. It is likely that triggering of effector functions is related to the concentration needed to initiate adhesion so bivalency increases the ability of immunoadhesins to selectively engage targets based on differences in epitope density.

We initially expected that previously reported difference in CD2 amount on naive and memory T cells might account for the selective depletion of memory T cells in patients treated with alefacept (4, 26). We found that naive, memory, *in vitro* activated effector T cells and Jurkat tumor cells all have approximately the same overall density of CD2 on the surface, and are equally sensitive to alefacept-mediated adhesion. The selective depletion of memory T cells that have been observed *in vivo* may reflect other properties like expression of other adhesion molecules or entry into particular microenvironments, for example, adhesion in the liver, which may result in selective depletion (33).

This study takes a step toward development of quantitative tools that can be applied to two-dimensional pharmacology. The basic experimental system and model can be applied to any antibody or immunoadhesin directly. There is no obvious barrier to replacing the Fc with another interacting domain to create completely novel bridging reagents to induce non-cytolytic regulatory interactions. This experimental platform and model could also be applied to multivalent nanoscaffolds with small modifications. The advantage of bivalency for receptor selectivity is likely to be a general characteristic of such scaffolds, which could then take advantage of low affinity small molecules by organizing them spatially for efficient bridging of cell surface receptors.

Acknowledgments—We thank Robert L. White III, Charles Spencer, Javier Satulovsky, and Anne Morawski for contributions to data collection and analysis. We thank R. Brown and J. Green for the CD16B-producing Jurkat cell line.

REFERENCES

1. Zettlmeissl, G., Gregersen, J. P., Duport, J. M., Mehdi, S., Reiner, G., and Seed, B. (1990) *DNA Cell Biol.* **9,** 347–353
2. Byrn, R. A., Mordenti, J., Lucas, C., Smith, D., Marsters, S. A., Johnson, J. S., Cossum, P., Chamow, S. M., Wurm, F. M., Gregory, T., Groopman, J. E., and Capon, D. J. (1990) *Nature* **344,** 667–670
3. Majeau, G. R., Meier, W., Jimmo, B., Kioussis, D., and Hochman, P. S. (1994) *J. Immunol.* **152,** 2753–2767
4. Ellis, C. N., and Krueger, G. G. (2001) *N. Engl. J. Med.* **345,** 248–255
5. van der Merwe, P. A., Barclay, A. N., Mason, D. W., Davies, E. A., Morgan, B. P., Tone, M., Krishnam, A. K. C., Ianelli, C., and Davis, S. J. (1994) *Biochemistry* **33,** 10149–10160
6. Dustin, M. L., Golan, D. E., Zhu, D. M., Miller, J. M., Meier, W., Davies, E. A., and van der Merwe, P. A. (1997) *J. Biol. Chem.* **272,** 30889–30898
7. Majeau, G. R., Whitty, A., Yim, K., Meier, W., and Hochman, P. S. (1999) *Cell Adhes Commun* **7,** 267–279
8. Galon, J., Robertson, M. W., Galinha, A., Mazieres, N., Spagnoli, R., Fridman, W. H., and Sautes, C. (1997) *Eur. J. Immunol.* **27,** 1928–1932
9. Dustin, M. L., Ferguson, L. M., Chan, P. Y., Springer, T. A., and Golan, D. E. (1996) *J. Cell Biol.* **132,** 465–474
10. Bromley, S. K., Iaboni, A., Davis, S. J., Whitty, A., Green, J. M., Shaw, A. S., Weiss, A., and Dustin, M. L. (2001) *Nat. Immunol.* **2,** 1159–1166
11. Weis, R. M., Balakrishnan, K., Smith, B. A., and McConnell, H. M. (1982) *J. Biol. Chem.* **257,** 6440–6445
12. Zhu, D. M., Dustin, M. L., Cairo, C. W., and Golan, D. E. (2007) *Biophys. J.* **92,** 1022–1034
13. Green, J. M., Schreiber, A. D., and Brown, E. J. (1997) *J. Cell Biol.* **139,** 1209–1217
14. Douglass, A. D., and Vale, R. D. (2005) *Cell* **121,** 937–950
15. Miller, G. T., Hochman, P. S., Meier, W., Tizard, R., Bixler, S. A., Rosa, M. D., and Wallner, B. P. (1993) *J. Exp. Med.* **178,** 211–222
16. Wells, A. F., Miller, C. E., and Nadel, M. K. (1966) *Appl. Microbiol.* **14,** 271–275
17. Dustin, M. L., Sanders, M. E., Shaw, S., and Springer, T. A. (1987) *J. Exp. Med.* **165,** 677–692
18. Kato, K., Koyanagi, M., Okada, H., Takanashi, T., Wong, Y. W., Williams, A. F., Okumura, K., and Yagita, H. (1992) *J. Exp. Med.* **176,** 1241–1249
19. Dustin, M. L. (1997) *J. Biol. Chem.* **272,** 15782–15788
20. Crothers, D. M., and Metzger, H. (1972) *Immunochemistry* **9,** 341–357
21. Klopfenstein, D. R., Tomishige, M., Stuurman, N., and Vale, R. D. (2002) *Cell* **109,** 347–358
22. Bell, G. I., Dembo, M., and Bongrand, P. (1984) *Biophys. J.* **45,** 1051–1064
23. da Silva, A. J., Brickelmaier, M., Majeau, G. R., Li, Z., Su, L., Hsu, Y. M., and Hochman, P. S. (2002) *J. Immunol.* **168,** 4462–4471
24. Liu, S. J., Hahn, W. C., Bierer, B. E., and Golan, D. E. (1995) *Biophys. J.* **68,** 459–470
25. Hibbs, M. L., Selvaraj, P., Carpén, O., Springer, T. A., Kuster, H., Jouvin, M. H., and Kinet, J. P. (1989) *Science* **246,** 1608–1611
26. Sanders, M. E., Makgoba, M. W., Sharrow, S. O., Stephany, D., Springer, T. A., Young, H. A., and Shaw, S. (1988) *J. Immunol.* **140,** 1401–1407
27. Dustin, M. L., Olive, D., and Springer, T. A. (1989) *J. Exp. Med.* **169,** 503–517
28. Zhang, Z., Zhang, M., Goldman, C. K., Ravetch, J. V., and Waldmann, T. A. (2003) *Cancer Res.* **63,** 6453–6457
29. Baselga, J., Albanell, J., Molina, M. A., and Arribas, J. (2001) *Semin. Oncol.* **28,** Suppl. 16, 4–11
30. Cartron, G., Dacheux, L., Salles, G., Solal-Celigny, P., Bardos, P., Colombat, P., and Watier, H. (2002) *Blood* **99,** 754–758
31. Louis, E., El Ghoul, Z., Vermeire, S., Dall'Ozzo, S., Rutgeerts, P., Paintaud, G., Belaiche, J., De Vos, M., Van Gossum, A., Colombel, J. F., and Watier, H. (2004) *Aliment Pharmacol. Ther.* **19,** 511–519
32. Uchida, J., Hamaguchi, Y., Oliver, J. A., Ravetch, J. V., Poe, J. C., Haas, K. M., and Tedder, T. F. (2004) *J. Exp. Med.* **199,** 1659–1669
33. Gong, Q., Ou, Q., Ye, S., Lee, W. P., Cornelius, J., Diehl, L., Lin, W. Y., Hu, Z., Lu, Y., Chen, Y., Wu, Y., Meng, Y. G., Gribling, P., Lin, Z., Nguyen, K., Tran, T., Zhang, Y., Rosen, H., Martin, F., and Chan, A. C. (2005) *J. Immunol.* **174,** 817–826
34. Williams, T. E., Nagarajan, S., Selvaraj, P., and Zhu, C. (2001) *J. Biol. Chem.* **276,** 13283–13288
35. Posner, R. G., Lee, B., Conrad, D. H., Holowka, D., Baird, B., and Goldstein, B. (1992) *Biochemistry* **31,** 5350–5356
36. Saffman, P. G., and Delbruck, M. (1975) *Proc. Natl. Acad. Sci. U. S. A.* **72,** 3111–3113
37. Schlessinger, J., Elson, E. L., Webb, W. W., Yahara, I., Rutishauser, U., and Edelman, G. M. (1977) *Proc. Natl. Acad. Sci. U. S. A.* **74,** 1110–1114
38. Winckler, B., Forscher, P., and Mellman, I. (1999) *Nature* **397,** 698–701
39. Meuer, S. C., Hussey, R. E., Fabbi, M., Fox, D., Acuto, O., Fitzgerald, K. A., Hodgdon, J. C., Protentis, J. P., Schlossman, S. F., and Reinherz, E. L. (1984) *Cell* **36,** 897–906
40. Shao, J. Y., Yu, Y., and Dustin, M. L. (2005) *Ann. Biomed. Eng.* **33,** 483–493